

Spatiotemporal-Correlation Analysis of Jet Noise from a High-Performance Military Aircraft

Blaine M. Harker,* Tracianne B. Neilsen,† and Kent L. Gee‡

Brigham Young University, Provo, Utah 84602

Alan T. Wall§

U.S. Air Force Research Laboratory, Wright–Patterson Air Force Base, Ohio 45433
and

Michael M. James¶

Blue Ridge Research and Consulting, LLC, Asheville, North Carolina 28801

DOI: 10.2514/1.J054442

Correlation analyses of ground-based acoustic-pressure measurements of noise from a tethered F-22A provide insights into the sound-field characteristics with position and engine condition. Time-scaled single-point (auto) correlation functions show that, to the side of the nozzle exit, the temporal-correlation envelope decays rapidly, whereas the envelope decays more slowly in the maximum radiation region and farther downstream. This type of spatial variation has been previously attributed to a transition from fine- to large-scale mixing noise in laboratory-scale jets. Two-point space–time (cross) correlation functions demonstrate that noise from a single engine operating at intermediate power is similar to that from a heated, convectively subsonic laboratory-scale jet, whereas additional features are seen at afterburner, relative to supersonic laboratory jets. A complementary coherence analysis provides estimates of coherence lengths as a function of frequency and location. Acoustic coherence lengths across the ground microphone array are used to analyze one-dimensional, equivalent-source-coherence lengths obtained from the DAMAS-C beamforming algorithm. The source coherence reaches its maximum downstream of the maximum source level, suggesting that uncorrelated sources meaningfully contribute to the dominant source region. In addition to revealing further the nature of the sound field near an advanced tactical engine, the characteristics seen should be useful as a phenomenological comparison point for those trying to model military-scale results both experimentally and numerically.

Nomenclature

A_{ab}	=	envelope function between measurements $a(t)$ and $b(t)$
D_j	=	jet-nozzle diameter
f	=	frequency
$G_{xy}(f)$	=	cross-spectral element between signals $x(t)$ and $y(t)$
$L_{\gamma^2}(x, f)$	=	coherence length
R_{xy}	=	correlation function between measurements $x(t)$ and $y(t)$
Sr	=	Strouhal number
t	=	time
z	=	downstream distance
γ^2	=	coherence
η	=	nondimensional timescale
τ	=	time delay

I. Introduction

CORRELATION analyses of near-field acoustical data from supersonic tactical aircraft engines provide key insights into the noise-field variation as a function of location and engine power. Furthermore, because jet-noise-source characteristics are imprinted on the radiated sound field [1], the spatiotemporal features found in the pressure field complement spectral analyses by providing a more complete understanding of the acoustic source, thereby assisting those who seek to more accurately replicate these environments analytically, numerically, and experimentally. For example, both two-point space–time pressure correlation functions [2–5] and the shape of single-point autocorrelation functions have been used to distinguish between the fine- vs large-scale nature of the jet-noise radiation [1,6]. These measurements have also been used to provide spatiotemporal length scales, either broadband [1] or band limited [7], which are useful in validating and improving jet-noise models [8–10]. Consequently, the correlation results presented in this paper for full-scale tactical engine noise extend the growing number of laboratory and computational jet studies that use auto- (single-point) and cross- (two-point) correlation functions of the acoustic field to obtain not only valuable information of the spatial structure of the noise field, but also insights into the noise sources found within the turbulent jet plume.

Previous experiments have used correlation analyses to relate pressure-field measurements to source phenomena. Early works by Clarkson [11], Fuchs [12,13], Maestrello [14], Fisher et al. [15], and Ribner [16], as well as a more recent work by Tam et al. [1], have suggested the autocorrelation function has significant negative loops when large-scale structure noise dominates the spectrum. This was verified by Harker et al. [6], who calculated autocorrelation functions defined by Tam's and Tam et al.'s large- and fine-scale similarity spectra [17,18], and showed that the autocorrelation function of the large-scale similarity spectrum contains significant negative loops. Viswanathan et al. [5] used an extensive conical array of microphones to calculate near-field correlation measurements of a laboratory-scale, heated supersonic jet. They determined that a large coherent

Presented as Paper 2015-2376 at the 21st AIAA/CEAS Aeroacoustics Conference, Aviation Forum 2015, Dallas, TX, 22–26 June 2015; received 1 May 2015; revision received 3 December 2015; accepted for publication 4 December 2015; published online 11 March 2016. Copyright © 2015 by the authors. Published by the American Institute of Aeronautics and Astronautics, Inc., with permission. Copies of this paper may be made for personal and internal use, on condition that the copier pay the per-copy fee to the Copyright Clearance Center (CCC). All requests for copying and permission to reprint should be submitted to CCC at www.copyright.com; employ the ISSN 0001-1452 (print) or 1533-385X (online) to initiate your request.

*Graduate Student, Department of Physics and Astronomy, N283 ESC. Student Member AIAA.

†Part-Time Assistant Professor, Department of Physics and Astronomy, N283 ESC. Member AIAA.

‡Associate Professor, Department of Physics and Astronomy, N283 ESC. Senior Member AIAA.

§Research Physicist, Battlespace Acoustics Branch, AFRL 711 HPW/RHCB.

¶Senior Principal Engineer, 29 N Market Street, Suite 700. Member AIAA.

region existed, at least two potential-core lengths downstream and beyond the maximum radiation region, as well as a single mechanism responsible for the generation and radiation of noise to the peak radiation sector. Kumar et al. [19] showed how the temporal width of the far-field correlation measurements broadened as a laboratory-scale jet was operated at under-, ideally, and overexpanded conditions. Liu et al. [20] calculated cross correlations as part of an analysis of numerical pressure fields resulting from simulations of perfectly expanded and underexpanded jets. They found that, although the broadband shock-associated noise (BBSAN) could be identified in the cross correlation, the autocorrelation distribution gives a more precise end location of the BBSAN. Correlation analyses, including the works of Panda et al. [21] and Papamoschou et al. [22], have also been applied to measure the correlation of pressure measurements in the acoustic field to the jet flow properties. The results of these prior correlation studies indicate that field characteristics can provide insights into source characteristics.

In this paper, the spatiotemporal-correlation and coherence analyses of sound measured in the vicinity of a static F-22A Raptor are presented to provide an improved characterization of the noise radiation, and to provide a benchmark case for comparing against modeling and laboratory-scale experiments. An introduction to correlation methods is followed by a short description of the experiment. Auto- and cross-correlation functions of the pressure field from an array of ground-based microphones in the vicinity of an F-22A aircraft at intermediate (INT) and afterburner (AB) conditions are presented to investigate the broadband features of the sound field. Some of the F-22A correlation features are not exhibited in previous laboratory-scale jet studies. To investigate these features further, a complementary study of the coherence of the noise at select frequencies is presented to provide additional insights, and allow for comparison between field properties and related source properties obtained using beamforming methods. Findings yield a more complete picture of tactical jet-noise characteristics and highlight features of noise from high-performance military aircraft that have not yet been replicated in laboratory-scale jets.

II. Methods

A short description of the methods for each of the correlation and coherence analyses applied to the F-22A data is provided in this section. First, definitions of the auto- and cross-correlation functions are followed by coherence spectrum and coherence-length definitions. Finally, a cross-beamforming and deconvolution algorithm called DAMAS-C is briefly described, and a method for extracting estimated source coherence from the DAMAS-C output is summarized.

A. Correlation

The single-point correlation (autocorrelation) functions are studied to understand the temporal scales over which the waveform is correlated and the evolution of these properties in space. In addition, two-point correlation (cross-correlation) functions provide a look at the spatiotemporal variation in the correlation properties, as well as estimates of correlation-length scales. The correlation between two waveforms is defined as [23]

$$R_{xy}(\tau) = E[x(t)y(t + \tau)] \quad (1)$$

in which the expectation value $E[\cdot]$ of a signal $x(t)$ with a signal $y(t)$ delayed by time τ . The autocorrelation function, $R_{xx}(\tau)$, is the inverse Fourier transform of the autospectral density, and there is, therefore, a single autocorrelation function that corresponds to a given spectrum. This property permitted the development of similarity autocorrelation functions from Tam's fine- and large-scale similarity spectra [6]. Similarly, the cross-correlation function, $R_{xy}(\tau)$, and the cross-spectral density form a Fourier transform pair. Although the correlation and the spectrum technically contain the same information, using one or the other can be beneficial in examining different trends in the sound field. For example, correlation may be used to more easily identify waveform periodicities, and obtain

spatiotemporal length scales and phase speeds. On the other hand, coherence (a normalized form of the squared cross spectrum) is useful for extracting the spatial phase relationships of the field as a function of frequency. In this paper, all correlation functions are normalized by the maximum correlation value (i.e., as correlation coefficients), such that $|R_{xy}(\tau)|^2 \leq R_{xx}(0)R_{yy}(0)$. In this study, a temporal or spatial correlation length is defined as the time or distance over which $\max[R_{xy}(\tau)] > 0.5$.

To facilitate the comparison of temporal decay rates of $R_{xy}(\tau)$ and better identify low-level features, the envelope function of the correlation coefficient is employed. The envelope function is defined as [23]

$$A_{xy}(\tau) = [R_{xy}^2(\tau) + \tilde{R}_{xy}^2(\tau)]^{1/2} \quad (2)$$

in which $\tilde{R}_{ab}(\tau)$ is the Hilbert transform of the correlation function. Because $A_{xy}(\tau)$ is positive semidefinite, it can be plotted on a logarithmic (decibel) scale to more clearly observe low-amplitude features not visible in $R_{xy}(\tau)$. Additionally, the envelope function is useful to more consistently quantify differences in the temporal decay rate of $R_{xy}(\tau)$ for various locations around a jet, or for jets of different scales and conditions. Instead of relying on an interpretation of negative loops in the autocorrelation to define a temporal or spatial correlation scale [1], $A_{xy}(\tau)$ provides the magnitude of the temporal correlation and can be used to compare the temporal decay of fundamentally different autocorrelation functions [e.g., $A_{xy}(\tau) > 0.5$] [6].

B. Coherence

The coherence between a reference microphone and other ground-array microphones indicates the spatial extent over which the individual frequency components of the jet noise are related, and allows for additional investigation of features seen in a broadband cross-correlation analysis. The frequency-dependent coherence function is defined as

$$\gamma_{xy}^2(f) = \frac{|G_{xy}(f)|^2}{G_{xx}(f)G_{yy}(f)} \quad (3)$$

in which the cross-spectral measurement $G_{xy}(f)$, relating signals $x(t)$ and $y(t)$, is normalized by the respective autospectra, and therefore, bounded between 0 and 1. In a manner similar to the correlation analyses, a spatial-coherence length, $L_{\gamma^2}(z_1, f)$, is defined as the length over which there is significant coherence. In this paper, it may be defined as the distance at which the coherence, $\gamma_{xy}^2(f)$, of a reference signal at z_1 drops below 0.5 when compared to adjacent measurements, z_i , in the upstream direction [7].

C. Source Coherence via Beamforming

Beamforming measurements have been used in multiple contexts in efforts to reconstruct source properties from jet-noise radiation [24–27]. Using phased arrays, pressure measurements provide equivalent-source reconstructions by defining a source-distribution region in the vicinity of the jet plume. Generally, beamforming analyses assume a distribution of incoherent simple sources. However, more advanced beamforming algorithms have been developed that successfully reconstruct spatially distributed sources with varying degrees of spatial coherence [28–30]. One such algorithm is an extension of the DAMAS [31] algorithm, known as DAMAS-C [32], which is favorable for jet-noise studies because of partial coherence over the source region as a function of frequency. A detailed description of the DAMAS-C algorithm can be found in [32]. Because flow parameters and refraction effects are not incorporated to the beamforming model presented, an equivalent-source region is obtained. Of importance here, however, is our use of DAMAS-C to provide an estimate of source coherence within the source reconstruction region. Although source level can usually be obtained as a function of space and frequency using traditional beamforming methods, DAMAS-C also determines a relationship in level and phase between two source locations, in which $X_{z_1, z_2}(f)$ represents the

DAMAS-C output due to the likelihood of sources at locations z_1 and z_2 along the jet centerline generating the measured pressure field. The algorithm is applied to each frequency component individually, and the coherence, $\gamma_{z_1 z_2}^2$, may be shown to be related by the corresponding beamforming outputs:

$$\gamma_{z_1 z_2}^2(f) = \frac{|X_{z_1 z_2}(f)|^2}{X_{z_1 z_1}(f)X_{z_2 z_2}(f)} \quad (4)$$

Thus, in addition to obtaining an estimated source region, the spatial properties of the equivalent-source coherence can also be obtained. In spite of this advantage, DAMAS-C has not been widely used because of its high computational expense, which requires on the order of N^4 operations, in which N is the number of beamforming reconstruction points. For the current work, a one-dimensional source distribution along the nozzle centerline axis, similar to other equivalent line-source models [15,24], is chosen with a 0.3 m spacing ($\sim 0.5D_j$) between each scan point, such that the algorithm run time for each frequency was reduced from days to minutes.

III. Experiment

In this section, details of the F-22A measurement [33] that are pertinent to the correlation and coherence analyses are provided. In addition, although engine operating parameters are not available, a discussion is included of how these results may possibly relate to published jet-noise studies for known operating conditions.

A. Full-Scale Measurement and Analysis

Noise measurements were made of a Pratt & Whitney model F119-PW-100 turbofan engine installed on Lockheed Martin/Boeing F-22A Raptor, which was tied down on a concrete run-up pad. One of the aircraft engines was operated at four engine conditions [idle, INT (80%), military (100%), and AB], whereas the other was held at idle. A linear array of 50 GRAS 6.35 and 3.18 mm type 1 microphones, spanning 30 m, was placed on the ground 11.6 m from the centerline of the jet axis, as shown in Fig. 1a. The ground-array element spacing was 0.61 m. Each measurement was taken for 30 s at either a 48 or 96 kHz sampling rate, depending on the engine condition tested, and each resultant waveform was divided into time-waveform blocks of

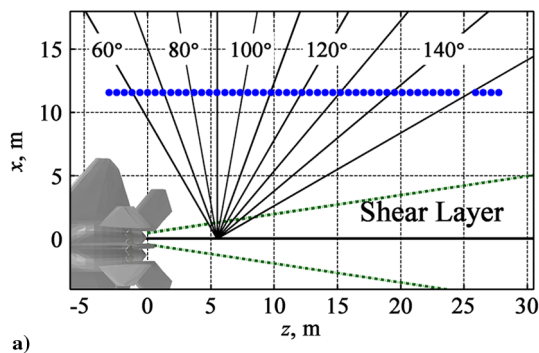


Fig. 1 a) Experimental setup schematic and b) photograph from F-22A Raptor test (ground array is along pavement edge).

2^{15} samples each with 50% overlap. A Fourier transform was applied to each block after a Hanning-window correction was applied, and cross-spectral calculations were averaged over the blocks to obtain cross-spectral density elements.

The one-third octave (OTO) band spectra of the F-22A measurement at INT and AB engine operation conditions are shown as a function of position z along the ground-based array in Fig. 2, and the averaged overall sound-pressure levels (OASPLs) across the array are plotted alongside. An extensive analysis of the spectral variation along the array, including contributions due to large- and fine-scale turbulent structures, is contained in [34]. The spectral comparisons show evidence that a combination of fine- and large-scale mixing noise exists over most of the spatial aperture at INT engine power, with the levels associated of the large-scale contributions remaining relatively flat. On the contrary, at AB condition, there is a more abrupt transition from fine- to large-scale contributions and a rapid increase in level due to Mach-wave radiation.

Also of importance here are the variations in peak frequency at each engine condition as a function of z . Sound to the sideline, defined as $4 \text{ m} < z < 6 \text{ m}$, and upstream ($z < 4 \text{ m}$) exhibits spectra that are broad in nature and generally contain a higher peak-frequency content (approximately 800–1200 Hz). Farther downstream, the peak frequency drops to between 100 and 200 Hz, and the spectral shapes narrow and become more haystacklike. Across most of the array, the spectral shape has a single peak frequency, as has been observed for laboratory-scale jets [5,27]. However, some locations exhibit a double-peaked spectral shape that appears as the peak shifts between two discrete frequencies. Such a transition region exists at both military and AB conditions in approximately the $12 \text{ m} < z < 15 \text{ m}$ range, in which two dominant frequencies exist in the spectra. Neilsen et al. [35] have described how the presence of dual spectral peaks is not accounted for by the analytical similarity spectral shapes given by Tam [17] and Tam et al. [18], and also

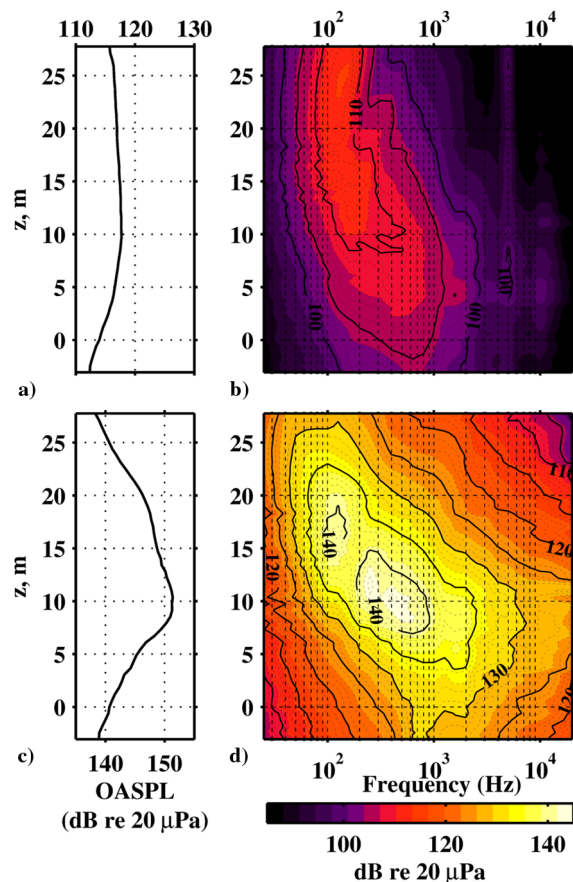


Fig. 2 Overall levels and OTO band spectra for ground-based microphones at a–b) INT and c–d) AB engine power.

discussed how these peaks are not present in existing laboratory-scale measurements. The reason for the double peaks in the military-jet-aircraft spectra is currently under investigation [36–38]. Note that a similar double peak has been observed in F-35 AA-1 data [39] and in far-field F-22A data [40], well below ground interference nulls caused by elevated microphones, and so this feature appears to be a characteristic of current-generation tactical aircraft noise spectra at high engine powers.

B. Comparison to Similar Experiments in the Literature

The correlation and coherence analyses add further dimensionality to prior jet-noise characterizations from this high-performance tactical aircraft. The previous investigations of the overall F-22A data set include near-field acoustical holography [41,42], vector intensity [43], beamforming [28], equivalent-source modeling [44,45], and similarity-spectrum analyses [34,35]. These studies have improved the understanding of military jet-noise environments, and elucidated both similarities and differences with laboratory-scale jets. Because the jet-nozzle exit conditions for the F-22A engine are not available, a complete scaling with laboratory studies is not possible. However, some basic scalings can be performed that establish a regime for this experiment and allow for connections with laboratory-scale phenomena.

Three scalings that potentially allow for, at the very least, phenomenological comparisons with laboratory-scale jets include jet-noise classification based on maximum radiation angle, scaling of peak Strouhal number in the maximum radiation direction, and geometric scaling based on nozzle diameter. First is the question of radiated overall directivity. As the convective Mach number of a heated jet transitions from subsonic to supersonic, the peak radiation angle shifts from 150 deg (re engine inlet) forward. For the INT engine condition (80%) here, the overall radiation angle is approximately 150 deg, suggesting the jet noise may be treated as being radiated from a convectively subsonic source. For the AB case, however, the maximum radiation angle is approximately 125 deg [40], indicating a convective Mach number of approximately 1.7–1.8. Note that these classifications are strengthened by a similarity-spectrum analysis [34] of the same data set. The analysis revealed a gradual transition between fine- and large-scale similarity spectra with increasing angle for INT power and a much more abrupt transition for AB. These similarity spectral trends were consistent with those of Tam et al. [1] for convectively subsonic and supersonic jets.

Although the F-22A engine jet conditions are unavailable, the derived convective Mach-number range exceeds prior scale-model engine tests. Greska [46] presented results from a laboratory jet that matched the operating conditions of the F404 engine, with a resulting far-field radiation angle of 130 deg. Baars et al. [47] described near-field correlation measurements of a heated supersonic jet that approximated the conditions of the F414 engine [48], resulting in the maximum overall level radiated at 135 deg. Other jet experiments, not intended to match tactical jet engines, but with maximum directivities in the 130–135 deg range, were Krothapalli et al. [49] and Baars and Tinney [50]. The former experiment was with a highly heated jet with conditions similar to the scaled F404/F414 engine tests, whereas the latter was with an unheated Mach 3.0 jet. Three laboratory-scale experiments with the convective Mach number required to produce a 125 deg peak far-field angle are noteworthy. Greska experimentally showed that the maximum directivity angle for supersonic jets shifted to 125 deg as temperature increased to beyond 1300 K for a jet Mach number of 1.3, and 1000 K for Mach 1.5 and Mach 1.8. The measurements of Seiner et al. [51] exceeded these jet velocities and temperatures, resulting in peak directivities at slightly lesser angles. Of particular relevance to this study, Viswanathan et al. [5] made near- and far-field correlation measurements of a heated supersonic jet with convective Mach number 1.69. Both the studies of Viswanathan et al. [5] and Baars et al. [47] will be described further as part of the data analysis.

The other potential scalings are related to frequency and geometry. For the AB case, the peak frequencies along the maximum radiation-

angle number are between 125 and 250 Hz. Prior engine tests, in which the supersonic jet conditions were available — for the F404 engine by Greska [46] and an advanced tactical engine by Schlinker et al. [26] — the peak Strouhal number is approximately 0.15–0.3. This suggests a frequency-to-Strouhal-number scaling of approximately $1.2E - 3 \text{ Hz}^{-1}$. Regarding geometric scaling, Tam and Zaman [52] suggest nonround nozzles may be considered as a round nozzle with equivalent area. Consequently, an approach to geometric scaling would be to treat the F-22A engine nozzle, despite its complexity, as a 2:1 aspect-ratio rectangle and a hydraulic diameter of 0.6 m [42]. These scalings, of course, have considerable uncertainty. Consequently, the figures in this paper will be presented in terms of dimensional length and frequency units; references to scaled units will be considered in the discussion as appropriate.

IV. Analysis and Discussion

We first present a broadband analysis of full-scale jet correlation measurements using auto- and cross-correlation techniques in Sec. II.A to obtain temporal and spatial waveform characteristics. This provides a general overview of the spatial variation in the waveform features and associated correlation lengths. Because many features within jet noise are frequency dependent, the correlation investigation is augmented by a coherence analysis in Sec. II.B, which provides spatial scales of frequency-separated elements. The resulting field-coherence maps provide estimates of the coherence lengths as functions of frequency and position for both engine conditions. Finally, because the connection between the field and source coherence is also of interest, equivalent-source-coherence measurements are obtained using the DAMAS-C beamforming algorithm and compared with the corresponding field-coherence measurements.

A. Correlation Analysis

The broadband nature of turbulent mixing noise is studied most easily using time-domain correlation analyses [53]. Previous work on laboratory-scale data provides a backdrop against which these correlation analyses are compared to indicate both the similarities and differences that exist between laboratory-scale and full-scale jet noise.

1. Autocorrelation Measurements

Several previous laboratory studies have used features of pressure autocorrelation functions to argue for the existence of large-scale and fine-scale turbulent structures as distinct sources of jet mixing noise. Tam et al. [1] state two arguments to distinguish between the two sources. First, the width of the peak in the autocorrelation is considerably narrower to the sideline than in the aft direction. This argument was used by Kumar et al. [19] and by Tam et al. [1,3] to indicate that large-scale turbulent structures generated the noise at the aft angles and that the randomness at sideline angles is indicative of fine-scale structures. However, it has been shown [6] that the autocorrelation-function width is strongly dependent on the spectral peak frequency, and scaling of the temporal axis by peak frequency causes the gross differences in the width of the autocorrelation function to disappear. Thus, the autocorrelation-function width is not intrinsically related to the nature of the jet-noise field, and a more careful analysis is required. The second argument by Tam et al. [1] is that the existence of negative loops (dips) in the autocorrelation at aft angles indicates the presence of partially correlated noise from the large-scale turbulent structures. Harker et al. [6] confirmed this to be true by demonstrating that the negative loops are present in the autocorrelation function obtained from the analytical similarity spectrum associated with the large-scale structures. A limited analysis of the autocorrelation of select F-22A waveforms indicated the presence of negative loops at downstream distances, similar to those seen in laboratory-scale cases [1,3,19]. However, there are features in the full-scale data that are not seen in the laboratory-scale cases.

Across the ground-based microphones in the vicinity of the F-22A, the autocorrelation functions show significant variation. As examples of the features seen at different locations, R_{xx} curves are shown in Fig. 3 for AB and microphones located at $z = 4, 12,$ and 26 m along the ground array. The left column displays the correlation as a function of delay time τ similar to Fig. 14 in Tam et al. [1], whereas those in the right column have been scaled by peak frequency: $\eta = \tau \cdot f_{\text{peak}}$. The initial positive peaks of the scaled autocorrelation functions have nearly the same width, but the widths of the Hilbert-transform-based envelopes, $A_{xx}(\eta)$, shown as dashed lines, illustrate the different natures of the sound measured at these three locations. The envelope for the sideline location ($z = 4$ m) has a narrower width, due to the broad spectrum and small-amplitude ringing that may result from BBSAN, given the similarity with the “wiggles” observed for an aerospike nozzle operated at off-design conditions by Kumar et al. [19]. At $z = 26$ m, the single set of deep negative loops in R_{xx} broadens A_{xx} , matching the observations of Tam et al. [1] for radiation dominated by large-scale noise. However, in the region of maximum OASPL, at $z = 12$ m, there are two sets of negative loops, which result in a different shape for A_{xx} beyond $\eta > 1$. This is a feature that has not been reported for laboratory-scale jet-noise studies. Overall, the differences in the autocorrelation functions in Fig. 3 imply that the noise signal characteristics vary at these three downstream distances.

The presence of these same features in the autocorrelation functions and envelopes over the entire 30 m spatial aperture reveals distinct transition regions between the types of signals for both INT (Fig. 4) and AB (Fig. 5) engine conditions. At AB, in Fig. 5, for locations with $z < 9$ m, there is only low-level ringing in the autocorrelation outside the peak region. When viewed in the time-scaled envelopes, the ringing corresponds to appreciable correlation, particularly for measurements in the sideline region. For $z = 9$ – 13 m, the second set of negative loops leads to a significant correlation over much greater values of η . It is important to note that this region corresponds to the maximum OASPL measured across the array, as seen in Fig. 2c, but slightly upstream of the dominant dual-peak region in Fig. 2d. For $z > 13$ m, the single set of negative loops is the only feature of significance outside the peak region. From the autocorrelation envelopes for the AB case, it can be seen that once the peak-frequency dependence is removed from the scaling, the relative temporal length of the negative loops does not increase significantly with downstream distance, suggesting an invariant nature to the

noise. Note that similar features are shown for military power in [54], that is, it is not solely an AB phenomenon.

To investigate if these autocorrelation characteristics are unique to high engine powers, they can be compared to the analysis for INT power that was shown in Fig. 4. The map of $R_{xx}(\tau)$ shows the lack of negative loops to the sideline with a gradual increase in depth in the downstream direction, but other distinguishing features are easier to see in $A_{xx}(\eta)$, which is shown on a decibel scale. There is less ringing for $z = 7$ m at INT than at AB, which is consistent with the hypothesis that the afterburning ringing at AB is due to BBSAN. For

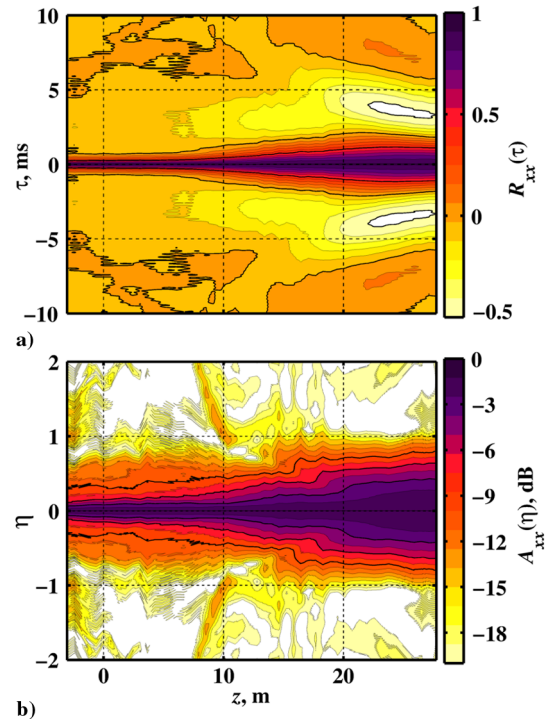


Fig. 4 a) $R_{xx}(\tau)$ at ground-based array for INT engine condition; b) Corresponding envelope functions, $A_{xx}(\eta)$, shown on a decibel scale.

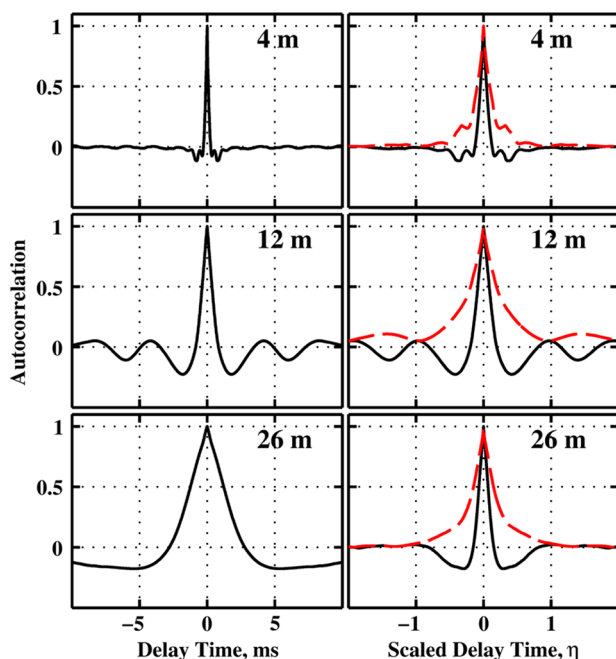


Fig. 3 Autocorrelation functions, $R_{xx}(\tau)$, (left) at different ground-based microphones for AB, and corresponding time-scaled versions, $R_{xx}(\eta)$, with overlaid autocorrelation envelopes (right).

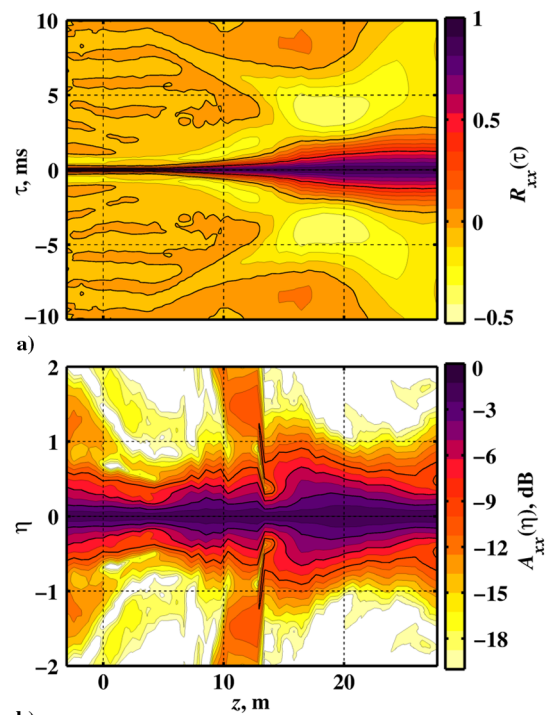


Fig. 5 Similar to Fig. 4 but at AB engine condition.

7 m < z < 11 m in Fig. 4, there is perhaps evidence of the double negative loops, albeit at levels about 10 dB down from the peaks. Farther downstream, the relative width of the envelope continues to increase, indicating that the relative temporal width of the single negative loops increases with distance downstream. This increase could be related to end-fire effects because of the large spatial aperture being considered. Thus, the fact that this broadening of the envelope is not observed at AB is even more meaningful: the signals received at the farthest downstream distances at AB have less evidence of the large-scale turbulent structures than those at z between 13 and 20 m.

To summarize the results of the autocorrelation analysis, the F-22A maps show both the similarities and differences with laboratory-scale jet noise. The presence of negative loops downstream, which are more quantifiable using envelope functions, helps to distinguish between large- and fine-scale turbulent mixing noise, and ringing in the upstream direction may be indicative of BBSAN at both scales. However, in between these two spatial regions, the double loops are unique to the full-scale jet-noise case, and although present at both engine conditions, they are significantly stronger at high engine powers.

2. Cross-Correlation Analysis

Some of the first studies to look at the spatial distribution of acoustic-pressure cross correlations were Clarkson's [11] and Maestrello's [14] work with subsonic jets. Clarkson explored the differences in the correlation for the hydrodynamic near field and the geometric near and far fields. Maestrello produced two-point space-time correlation maps (correlograms) over a distant sphere to illustrate the usefulness of acoustic-pressure correlations in quantifying the broadband features of the jet noise. Maestrello's goal was to use the phase-preserving cross-correlation functions as an inverse problem for identifying source characteristics. Although his conclusions were not universally accepted [16], Maestrello concluded that the lack of correlation at angles to the side of the nozzle exit was indicative of incoherent sources and that larger regions of high cross-correlation peaks for angles closer to the jet axis were indicative of a more coherent source downstream than near the nozzle exit.

The cross correlation of the acoustic-pressure field has been used in recent years to show support for the two-source model of jet noise proposed by Tam et al. [18] based on the presence of uncorrelated fine-scale turbulent structures radiating to the sideline and partially correlated large-scale turbulent structures responsible for the Mach-wave radiation in supersonic jets. The angular variation in cross correlations for a wide variety of subsonic and supersonic laboratory jets has confirmed what Maestrello [14] originally observed: for angles close to the jet axis, there is relatively high correlation. Conversely, for sideline angles, the peak cross-correlation values drop off rapidly [1,2,4,5,55]. A study by Ahuja et al. [2] has shown the same trends for a nozzle of a variety of shapes, including a rectangular nozzle with an aspect ratio of 8. These overall features have appeared to be relatively independent of the jet velocity for measurements in the acoustic far field [5].

The analysis of the cross-correlation functions from the 50 ground-based microphones provides the unique opportunity to examine if the noise in the vicinity of the F-22A exhibits similar temporal and spatial evolution as laboratory jets or, if like autocorrelation analysis, there are significant differences. Examples of the normalized cross-correlation coefficient, R_{xy} , are displayed for AB in Fig. 6 for reference microphones at $z = 4, 12,$ and 26 m, and the closest four microphones on either side (spaced at 0.6 m (2 ft) intervals, except for one 1.2 m (4 ft) gap [seen in the bottom plot]). There is essentially no correlation ($R_{xy} < 0.1$) between the microphone at $z = 4$ m and the neighboring microphones. At $z = 12$ m, which is within the maximum OASPL region, the peaks in the cross correlation fall off more gradually and exhibit a second set of negative loops, similar to the autocorrelation. At $z = 26$ m, the maximum values of cross correlation are significantly greater, and the cross-correlation functions are broader and contain a single negative loop, similar to the findings of previous studies. As with the autocorrelation, some of the

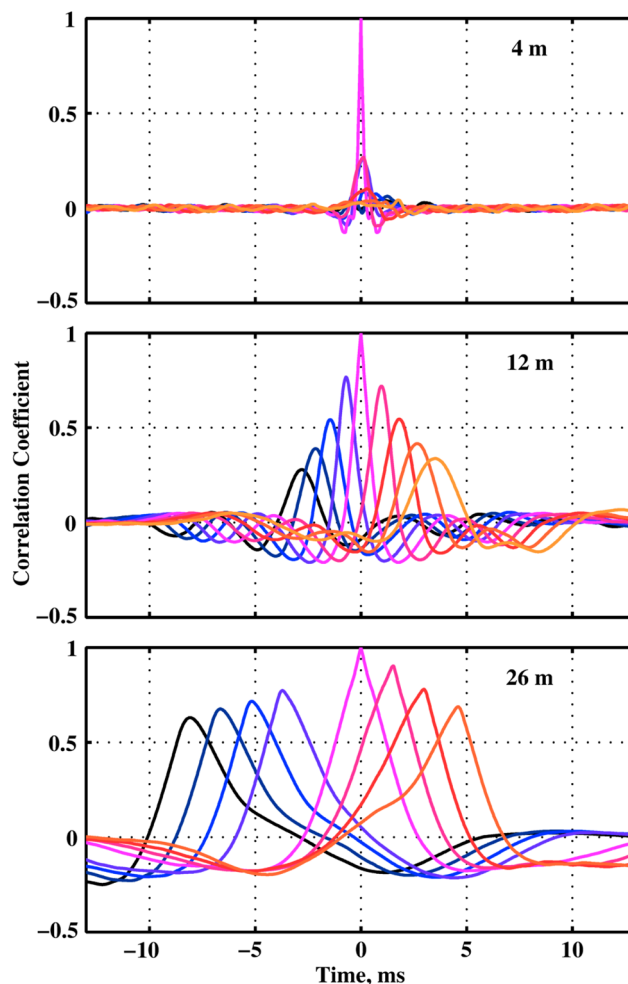


Fig. 6 Autocorrelation and neighboring cross-correlation functions at AB, with reference microphones located at downstream distances of 4, 12, 26 m.

broadening in the cross correlation as downstream distance increases is caused by the decreasing peak frequency. However, because the cross correlation involves two signals, the most meaningful frequency scaling to correct for the change in peak frequency has not yet been determined.

The spatiotemporal interdependence between the recorded signals can be seen in correlograms that have been calculated across the entire array, relative to the same three reference microphones. The correlograms are shown in Fig. 7 for INT power and Fig. 8 for AB engine condition. As with the autocorrelation, the use of the Hilbert-transform-based envelopes of the cross correlation allows the correlograms to be plotted on a logarithmic scale, facilitating the identification of low-level features. At INT (Fig. 7), the magnitude and extent of the region of large correlation in $A_{xy}(\tau)$ increase when the reference microphone is located farther downstream. However, for all three reference locations ($z_{\text{ref}} = 4, 12,$ and 26 m), there is appreciable correlation across the array, indicating that partially correlated noise exists across the entire 30 m aperture. This is likely due to the large spatial region over which the large-scale turbulent mixing noise contributes significantly to the signals, as shown via spectral decomposition in [34]. The turning points with zero slope in Fig. 7 mark the region at which acoustic energy is traveling perpendicular to the array and the transition between the upstream and downstream radiation. For the INT case, this turning point occurs between $z = 0$ and 5 m in all three correlograms, suggesting that the overall source location is close to the nozzle exit ($< 8D_j$). In addition, the slope of the correlation functions at downstream locations is relatively constant, indicative of planar wave fronts crossing the array with an apparent directivity of 145–150 deg. This directivity is consistent with a heated, convectively subsonic jet [26]. Constant

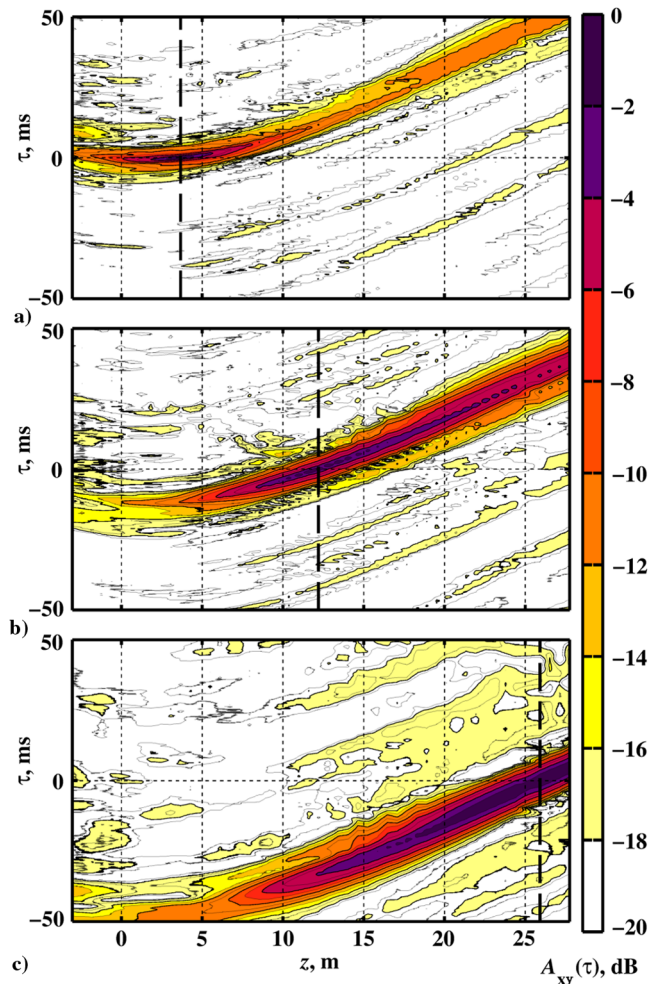


Fig. 7 Envelope-based cross correlograms, $A_{xy}(\tau)$, at INT; reference microphones are located at downstream distances of 4, 12, 26 m.

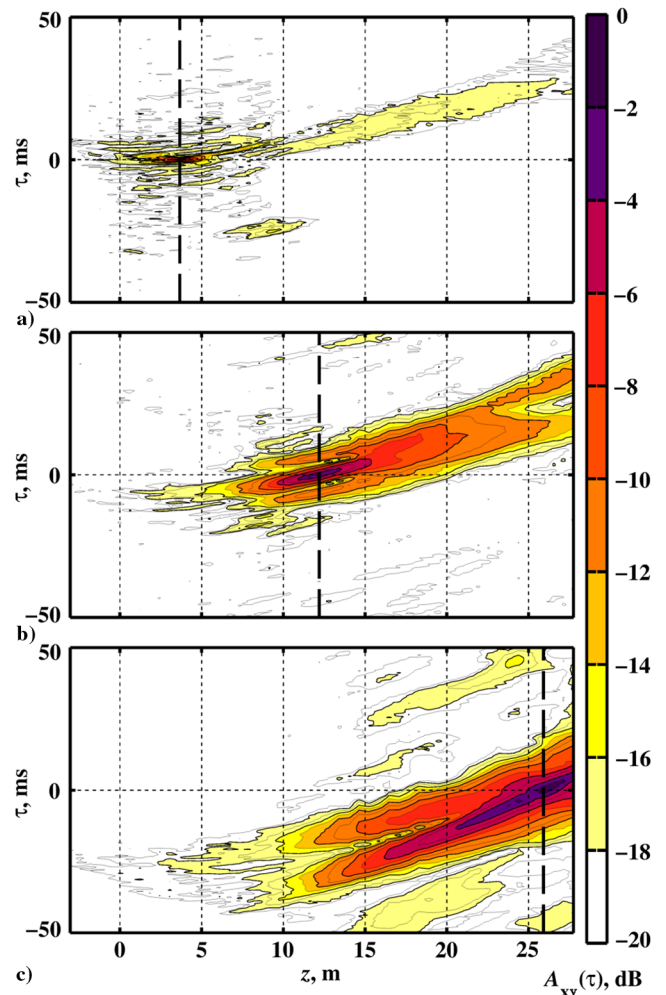


Fig. 8 Similar to Fig. 7 but at AB engine condition.

downstream slope for a space–time correlogram across a linear array was used previously by Baars et al. [47] to calculate the phase speed across a linear array located near an unheated jet.

The correlograms for the AB in Fig. 8 vary greatly from those seen in the INT case. The high correlation region depends greatly on the location of the reference microphone z_{ref} . When $z_{\text{ref}} = 4$ m (Fig. 8a), there is little cross correlation with the other locations and a relatively compact turning point ($3 \text{ m} < z < 5 \text{ m}$), both of which are indicative of uncorrelated noise dominating the noise radiation in this region. The turning points for downstream reference microphones are more extended, $3 \text{ m} < z < 7 \text{ m}$, and the slope of the region of large correlation is not constant, but continues to increase, both of which could be indicative of the extended nature of the source. Note that changing cross-correlogram slopes have been previously used within the hydrodynamic near field to estimate the decay rate of convective velocities along the shear layer [47].

Additional correlogram features are present for downstream reference microphones at AB that are not observed at the sideline or at any locations in the INT case or in laboratory studies. When $z_{\text{ref}} = 12$ m, within the region of maximum OASPL between 10 and 15 m (see Fig. 8b), there is essentially no correlation with the upstream locations ($z < 5$ m), and a relatively large aperture of high correlation in the downstream direction. In addition, there are striations in the cross correlations near $z_{\text{ref}} = 12$ m and at the farthest downstream locations. This splitting of the region of high correlation is seen more clearly in Fig. 8c. The signals recorded in the region of maximum OASPL have significant correlation with the signal at $z_{\text{ref}} = 26$ m at two different time delays. The slopes of the two curves in the array correspond to two sets of waves with discretely different phase speeds propagating through the array, resulting in different far-

field directivities. This dual directivity has been noted in other studies of the F-22A data [34,38,43]. Tam and Parrish [37] have postulated that one of these sources is associated with indirect combustion noise and the other with large-scale turbulent mixing noise. However, it may be significant to note that, in the correlograms, both branches appear to have turning points at $z \sim 5$ m, suggesting that the apparent overall origins of both the noise sources are at least that far downstream. Alternatively, Liu et al. [36] observed that for high-temperature jets, such as those found in full-scale military applications, large-eddy simulations showed a separation of two noise components which radiate in a similar direction in low-temperature jet cases. They hypothesized that the Mach wave radiation and the large-scale turbulent structures radiation are distinct components and thus responsible for the separate radiation angles. In any case, further investigation is required to identify the underlying mechanisms.

The differences between INT and AB are also evident in the spatial distribution of the maximum cross-correlation coefficients between all 50 microphones. To facilitate discussing the features of the peak correlation values, correlation lengths are defined as the distances over which the $R_{xy} > 0.5$, shown by the bold contour line in Fig. 9. Considering INT power in Fig. 9a, the small correlation lengths at sideline locations indicate the presence of relatively uncorrelated noise, with correlation increasing in the downstream direction. This behavior is phenomenologically similar to laboratory-scale jets [1,5], but acoustical cross-correlation lengths appear not to have been quantified for laboratory jets previously. For AB, however, the spatial distribution of the peaks of the correlation functions has somewhat different features. First, for $z_{\text{ref}} < 7$ m, the correlation lengths are less than the microphone spacing of 0.6 m, and are overall shorter than for INT, even beyond $z_{\text{ref}} = 20$ m, where the peak frequency for AB

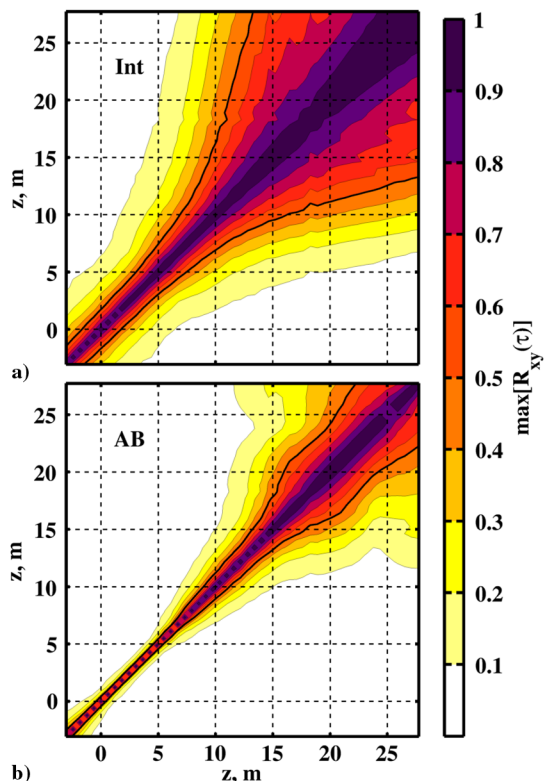


Fig. 9 Maximum cross-correlation coefficients for a) INT and b) AB condition.

begins to dip below INT. Viswanathan et al. [5] noted a reduction in peak correlation by nearly 50% as Mach number increased from a convective Mach number of 1.05 to 1.69 for highly heated jets, and so these results are not surprising. However, the cause for the dip in correlation length at around $z_{\text{ref}} = 22$ m for Fig. 9 is undetermined. It corresponds to a relatively rapid change in OASPL in that region, and so perhaps could represent a transition away from the dominant Mach-wave-radiation region to other large-scale radiation phenomena that dominate beyond 25 m downstream. However, corroborative experiments are required to verify this hypothesis.

B. Coherence Analysis

Coherence is useful to characterize the directivity and propagation of jet-noise data based on frequency-dependent characteristics, and thereby directly complements the correlation analyses. The coherence across the linear array, located in the geometric near field of the F-22A, is used to explore the properties of the sound field. In addition, a cross-beamforming technique yields an estimate of the coherence properties of an equivalent one-dimensional source located along the jet centerline. A comparison between the field coherence and the estimated source coherence provides additional insight of the jet noise dependent on the engine condition.

1. Field Coherence

Previous coherence studies of laboratory-scale jets provide a background against which the full-scale coherence can be evaluated. For example, Baars et al. [47] calculated the coherence spectra at multiple reference locations for a heated, supersonic jet. They showed high spatial coherence across a linear array in the hydrodynamic near field, with coherence lengths, L_{γ^2} , up to $7D_j$, particularly at frequencies associated with Mach-wave radiation. Work by Viswanathan et al. [5] showed both the azimuthal and axial variations of coherence as a function of frequency for heated subsonic and supersonic jet-noise conditions. Although sideline coherence lengths were small, they found a large coherent region about two potential-core lengths downstream that was about $15D_j$ in length, and which demonstrated high azimuthal coherence. Further work

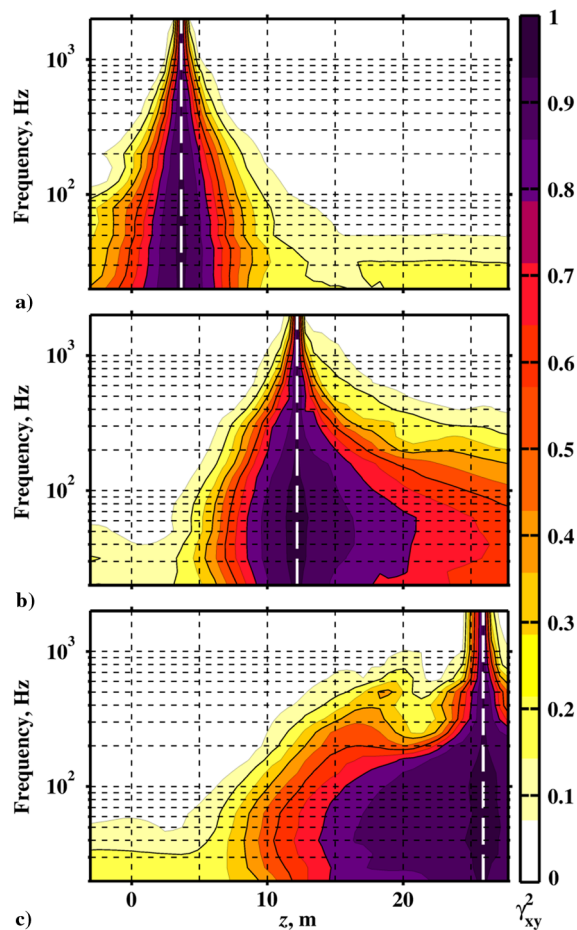


Fig. 10 Coherence spectra at INT for reference microphones at a) 4, b) 12, and c) 26 m.

done by Ahuja et al. [2] showed the coherence of subsonic and supersonic unheated jets in the far field. They found, similar to Viswanathan et al. and similar correlation studies, that for both subsonic and supersonic cases, there are high degrees of coherence in the downstream direction, and incoherent noise in the sideline and upstream direction at most frequencies. However, they also observed nonnegligible coherence between the sideline and downstream measurements for $Sr < 0.1$.

In this study, the coherence analyses of INT and AB power conditions are presented, which show both similarities and differences with the laboratory-scale measurements described previously. In addition, coherence lengths show the effects of different mixing noise contributions in the measurements, as the fine-scale and large-scale turbulent mixing noise have short and long coherence lengths, respectively. These coherence-length estimates near the F-22A across downstream distance, frequency, and engine condition can enhance jet-noise prediction models and design of measurement arrays.

Coherence calculations have been performed for the ground-based array as described in Sec. II, and are shown at OTO band center frequencies for reference locations $z_{\text{ref}} = 4, 12,$ and 26 m in Fig. 10 for INT power and Fig. 11 for AB power. For both engine conditions, the coherence spectra for $z_{\text{ref}} = 4$ m (Figs. 10a and 11a) are highly symmetric spatially in the upstream and downstream directions, with the exception of frequencies below 50 Hz. This low-frequency observation agrees with the findings of Baars et al. [47] for a laboratory-scale engine experiment. When the reference microphone is placed in the region of maximum OASPL, (about 10–25 m at INT and 10 m for AB), the coherence transitions dramatically to be highly coherent at most frequencies below 400 Hz ($Sr < \sim 0.5$) in the downstream direction, although the region of high coherence does not extend in the upstream direction. Thus, for example, the 100 Hz coherence lengths at INT condition in Fig. 10b extend up to 15 m in

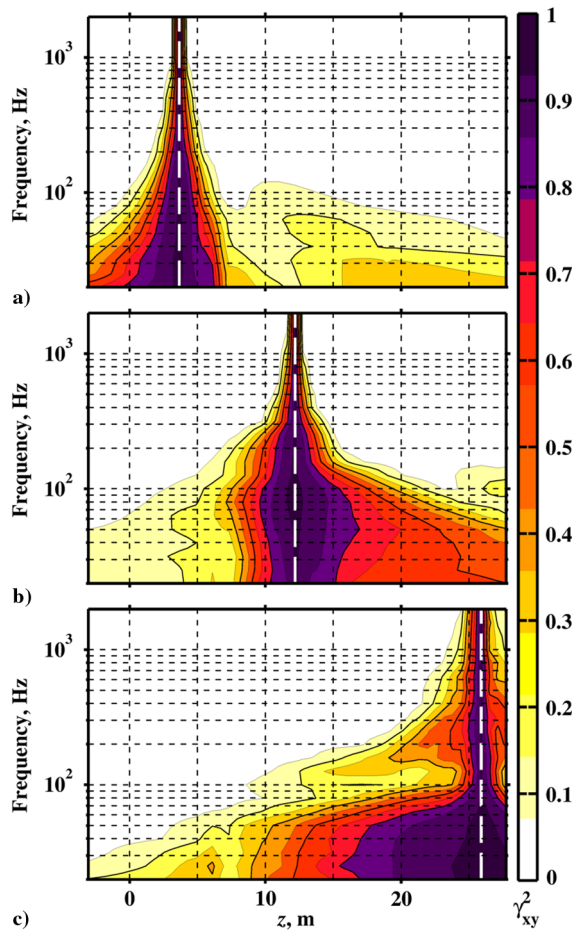


Fig. 11 Similar to Fig. 10, except at AB condition.

the downstream direction, but only about 5 m in the upstream direction. This highly self-coherent region, ascribed to the large-scale radiation features, has been observed by Baars et al. [47] for a supersonic heated jet, and by Viswanathan et al. [5] for both subsonic and supersonic heated jets. However, this large downstream coherence region is most dominant for frequencies below 400 Hz, as, similar to sideline measurements, the coherence is much more spatially symmetric at higher frequencies. The AB case shares similar general features with the INT, except that L_{γ^2} values progressively decrease as the engine power increases. The distinguishing features in the spatial dependence of coherence length across engine conditions are few: the onset of high L_{γ^2} values at AB occurs slightly upstream compared to the INT case — consistent with the idea that large-scale structure radiation shifts upstream with the increase in engine power (convective Mach number) [33], and at $z_{\text{ref}} = 26$ m (Fig. 11c), the coherence at 100 Hz is markedly low at AB for unknown reasons.

The spatial-coherence characteristics shown in Figs. 10 and 11 can be summarized using coherence lengths, which quantify the spatial and frequency-dependent variation in the coherence of the sound field. These are shown in Fig. 12, with L_{γ^2} representing the coherence lengths in the upstream direction relative to the reference position. Because of the way the coherence length is calculated, good estimates of upstream coherence lengths are not available when the array does not extend sufficiently far to capture the location at which $\gamma^2(f) \leq 0.5$. These regions are shaded out in the figure. As seen in the previous figures, coherence lengths generally decrease with increasing engine condition, and they are generally largest in the downstream direction where large-scale-structure turbulent mixing noise dominates. The coherence lengths also highlight less obvious features in sound field. For example, for both engine conditions, the variation in L_{γ^2} is seen to be very pronounced for frequencies below 200 Hz and changes rapidly for $z_{\text{ref}} > 10$ m. This corresponds to the

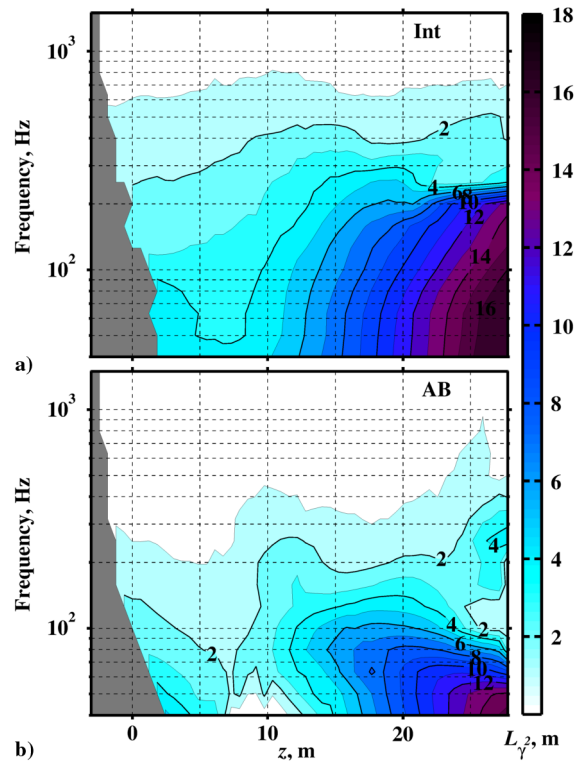


Fig. 12 Coherence lengths, L_{γ^2} , for a) INT and b) AB power.

regions where the maximum overall levels occur, as shown in Fig. 2, and where the spectral shapes are well described by solely the large-scale turbulent-structure similarity spectrum [34]. In the AB case, a small increase in L_{γ^2} values is visible, between $125 \text{ Hz} < f < 400 \text{ Hz}$ and at $z_{\text{ref}} = 11 - 12$ m. Considering spectral levels in Fig. 2, this corresponds to the dominant spectral features across the array between $200 < f < 500 \text{ Hz}$. Thus, the coherence lengths of the primary radiation at these frequencies are significant, although much lower in comparison with the coherence lengths farther downstream [e.g., $L_{\gamma^2}(125 \text{ Hz})$ at $z_{\text{ref}} = 17$ m]. In addition, a transition region exists, in which L_{γ^2} values indicate a dip in coherence lengths. At both engine powers, this dip occurs for $40 \text{ Hz} < f < 125 \text{ Hz}$ and at $z_{\text{ref}} \sim 7 - 8$ m, dependent on frequency. It was previously shown that a combination of the fine-scale and large-scale similarity spectra is necessary to represent the measured spectra in this region [34]. In addition, the frequencies at which the dip in coherence length occurs coincide with the locations where the two spectra are equal contributors to the spectral levels.

To further investigate the spatial variation in coherence lengths near the peak frequency, the coherence at two particular frequencies is examined at AB condition between all microphones on the ground-based array in Fig. 13. Coherence plots are oriented, such that self-coherence (nominally unity) occurs along the diagonal, and coherence between two distinct locations can be found along the off-diagonal elements. Shown alongside the coherence maps are the corresponding sound-pressure levels (SPLs) across the array at each frequency. The largest levels generally correspond to locations with the longest coherence lengths. However, this does not seem to be the case in the upstream direction. At 100 Hz, a narrower spatial extent of significant correlation is located at $z = 6 - 7$ m, separating larger coherence lengths in the far downstream and the upstream direction. This is also present at 200 Hz, although more difficult to observe. In this region, the SPL increases with z , but the coherence lengths unexpectedly decrease to a minimum value. The minimum coherence levels may result from the interference of competing independent sources. Previous work showed that the spectral shapes along the ground-based array change from matching the general features of the fine-scale similarity spectrum to those of the large-scale similarity spectrum over a transition (or combination) region that occurs over $z = 5 - 7$ m for frequencies below 400 Hz [34]. The presence of

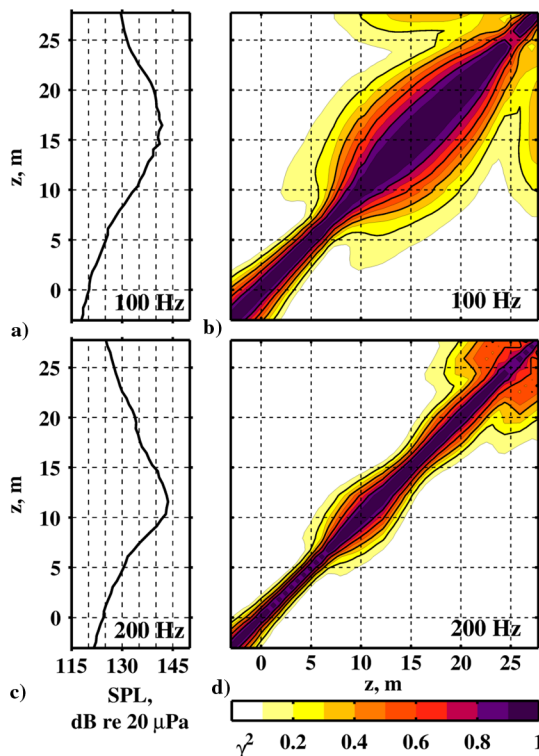


Fig. 13 Sound pressure measurements and corresponding spatial coherence at AB power for a–b) 100 Hz and c–d) 200 Hz.

similar levels of the independent fine-scale and large-scale turbulent mixing noise would account for the drop in coherence in this transition region. Thus, the independent signals would be responsible for increasing overall levels, and yet decreasing coherence lengths in this region. Although some have recently discounted the two-source model of jet noise [1,55] in favor of continuous source models, such as a wave-packet ansatz, the similarity-spectrum fit performed independently nevertheless explains the otherwise discrepant effects seen here in the coherence at the sideline.

In addition to the large spatial coherence related to the Mach-wave radiation, there is a secondary region of large spatial coherence in the far downstream region of the array ($z > 20$ m), visible in Figs. 13b and 13d. At 100 Hz, the spatial extent of this region extends up to 15 m, although coherence levels are lower ($0.1 < \gamma^2 < 0.4$) compared with the 200 Hz measurements ($0.1 < \gamma^2 < 0.7$), in which the spatial extent is smaller (about 5 m). Interestingly, this region is also separated from the coherence associated with Mach-wave radiation by a region of low spatial coherence, similar to the effect seen at $z = 6 - 7$ m, suggesting an independent signal radiating in the far downstream direction. Tam and Parrish [37] argued that farther aft of the Mach-wave radiation, there is evidence in the spectral data of radiation from an additional source in the AB condition for these frequencies. This needs to be the subject of further study. There is also evidence related to the dual spectral peaks at this engine condition seen in Fig. 13d as an additional narrowing of the correlation lengths for $15 \text{ m} < z < 20 \text{ m}$. The previous cross-correlation analysis showed evidence corresponding to two radiating sources with different directivities at AB. This is related to the dual spectral peaks that are seen in Fig. 2 and that are just visible in the levels in Fig. 13c. Although these two features are relatively self-coherent, coherence between the two peaks is only minimally significant. These radiators may thus be independent and associated with two incoherent sources. The coherence relating these features is explored in greater detail through holography analyses in [38].

2. Source-Coherence Analysis

The analyses thus far have characterized the correlation and coherence properties of the acoustic field, which provides insights about the nature of the source. However, source-related character-

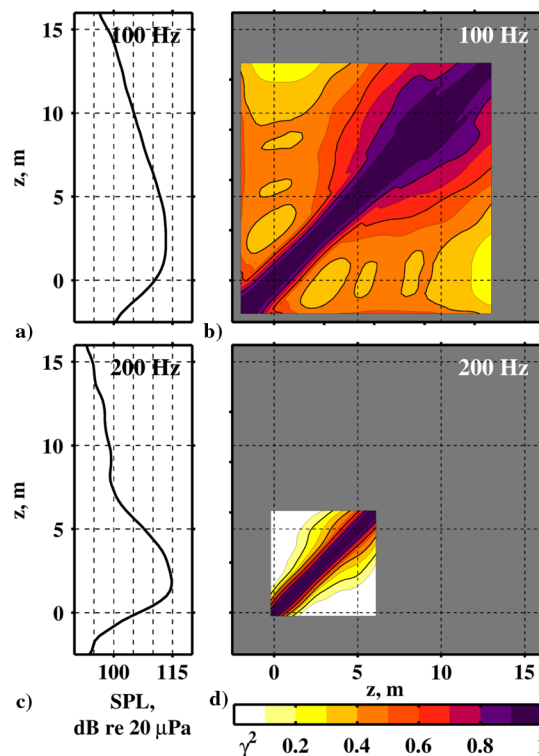


Fig. 14 Beamforming levels and corresponding coherence of equivalent sources from DAMAS-C for INT power at a–b) 100 Hz and c–d) 200 Hz.

istics can be obtained more directly from pressure data, even in the absence of flow information. For example, Baars et al. [47] used a linear microphone array located within the hydrodynamic near field of their F414-simulated jet to show a significant decrease in the convective (phase) speeds between 11 and $20D_j$ downstream of the nozzle exit, which they attributed to the decay of large-scale turbulent structures. Others have shown direct correlation between the flow- and acoustic fields. For example, Papamoschou et al. [22] found a significant correlation between beamformed far-field acoustic-pressure and jet shear-layer optical deflectometry measurements in the mixing region and outside the hydrodynamic layer. Panda et al. [21] correlated far-field acoustical pressure with jet density and velocity measurements for subsonic and supersonic unheated jets at laboratory scale. They found that correlation between density and velocity parameters was greatest in the downstream radiation, corresponding to large coherent structures.

The prior studies show direct links between the correlation properties of the radiated acoustic field and the source. Here, in the absence of flow data, the coherence properties of the source are obtained by beamforming the ground-array pressure measurements to the jet centerline. Because the DAMAS-C algorithm used (see Sec. II) makes no assumptions on the degree of source correlation, source-coherence properties can be calculated as part of the analysis. The source-coherence maps are shown in Fig. 14 for INT power and Fig. 15 for AB at 100 and 200 Hz, with the beamformed source levels plotted alongside. Coherence values are only shown for estimated source amplitudes within 12 dB of the maximum reconstructed level. The diagonal elements of the coherence maps represent the self-coherence at each reconstruction location, which by definition is unity. The off-diagonal elements, $\gamma_{z_1 z_2}^2$, represent the coherence between equivalent sources located at positions z_1 and z_2 along the jet centerline.

There are a number of noteworthy features in the source-coherence results in Figs. 14 and 15. First, generally speaking, the calculated source coherence contracts with increasing frequency as well, similar to the trends seen in the field measurements. At 100 Hz, the spatial aperture of significant coherence is particularly large at both engine conditions, with source-coherence lengths ($\gamma^2 > 0.5$) that span 5–6 m ($8-10D_j$) for the AB case within the peak source region. This lends merit to efforts to produce self-coherent (e.g., wave packet) models to

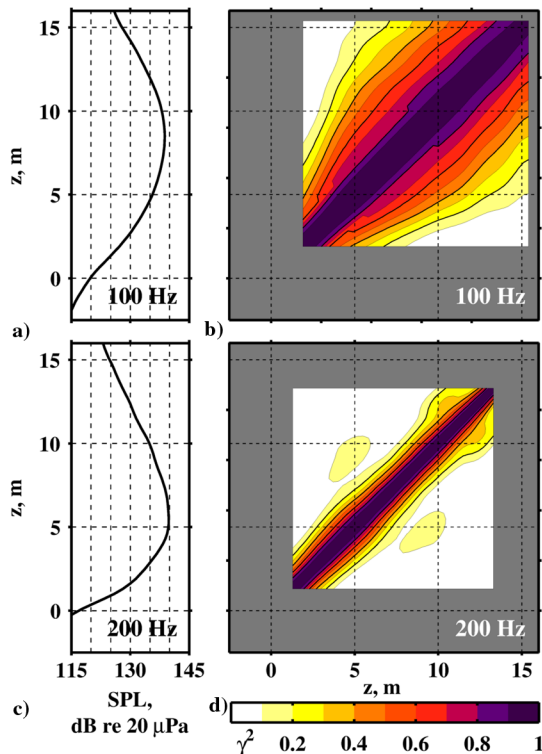


Fig. 15 Similar to Fig. 14, except at AB power.

characterize the radiation in the large-scale radiation regions. Second, the dual radiation lobe for AB at 200 Hz that produced two coherent regions in Fig. 14 has resulted in a single broad source region with maximum coherence in the 5–9 m range. Recent holography source reconstructions for the F-22 have shown that the dual radiation lobe in the field collapses to a single source region, but which extends over multiple axial coherence lengths [56].

A final feature of note in the beamforming source-coherence maps in Figs. 14 and 15 is the fact that, for both engine conditions, the region of maximum coherence is downstream of the maximum amplitude, with the difference being greater for INT than AB. This could be possibly related to the laboratory-scale findings of Viswanathan et al. [5], who showed that, for their test with convective Mach number 1.69 (thus approximating AB here), the radiation far downstream was most correlated with near-field measurements between 13 and 31 D_j . Jordan and Colonius [53] later countered these conclusions, suggesting that tracing their results back to the centerline results in a coherent-source region that was both farther upstream and smaller. The conflicting views merit a further look. In the Viswanathan et al. test, the peak overall directivity of the jet was approximately 125 deg, and the region of maximum correlation was in the 135–150 deg range. Although correlation is a broadband quantity, the tie between the aft angles and the downstream location suggests that the high correlation is due to low frequencies (i.e., $Sr < 0.1$) that have downstream source origins relative to the overall dominant radiation region. However, ray tracing their results back to the centerline would, as Jordan and Colonius pointed out, contract their results.

For the results here, we recall that 100–200 Hz is in the peak-frequency range of the spectrum in the maximum radiation direction for both engine conditions. At AB, these frequencies are believed to fall in the $Sr \sim 0.15 - 0.3$ range, not the low frequencies that Viswanathan et al. [5] were likely considering. Through ray tracing, the maximum directivity angles can be used to relate the levels at the ground array and the source, but can also be used to show that the maximum coherence at a given frequency does, in fact, appear downstream of the maximum source level. These results, and the fact that the difference is greater for INT than for AB, can be explained with a two-source model of jet noise — a relatively compact, uncorrelated source region and an extended, correlated source region,

like the fine- and large-scale structures described by Tam et al. [1]. The field analyses already have distinguished between fine- and large-scale behavior, showing relatively uncorrelated noise to the sideline and correlated noise downstream. For each frequency, however, the source regions will overlap, thus producing a maximum level that may result upstream of the maximum coherence, which is dominated by the extended source producing the downstream radiation. The fact that the spatial difference is greater for INT than AB would then be attributed to the fact that the fine- and large-scale contributions are more equal for INT than for AB, which was shown previously through a similarity-spectrum analysis [34].

V. Conclusions

A detailed time-waveform analysis of jet noise from a high-performance military aircraft has been completed. Correlation and coherence analyses have been presented from ground-array data collected in the vicinity of a tethered F-22A with a single engine operated at INT and AB engine conditions. The comparison of the combined analyses with previously published studies has confirmed that many of the basic properties of laboratory jets are phenomenologically the same as those observed for noise from the F-22A. All the analyses indicate that the noise radiated at INT power seems to behave largely like a heated, convectively subsonic jet with uncorrelated, fine-scale turbulent mixing noise to the sideline and with a smooth transition to more correlated, large-scale mixing noise downstream. However, for the AB jet, the analyses contain features that have not been observed for laboratory-scale jets.

The fundamental differences between the correlation functions of high-power full-scale and convectively supersonic laboratory-scale jets appear in the region of maximum OASPL. Autocorrelation functions reveal a secondary set of negative loops in this region, whereas laboratory-scale jets have only shown no loops to indicate fine-scale noise or a single set of loops to indicate noise associated with large-scale structures. In the cross-correlation analyses, the dominant features in the correlograms appear to split around and downstream of the dominant radiation direction, thus correspond to multiple phase speeds across the array. Both analyses are indicative of multiple, mutually incoherent radiating sources with distinct directivity patterns that contribute to the sound radiation in the region of maximum overall level, resulting in dual-peaked spectral shapes and dual directivity lobes.

Two complementary coherence studies have also been presented. First, the field-coherence spectra and corresponding coherence lengths found at INT and AB exhibit properties similar to those observed for laboratory-scale jets, with a reduction in coherence length at frequencies in which there are believed to be nearly equal contributions from fine- and large-scale structures [34]. For the AB case, however, there are additional increases and reductions in coherence length in the downstream direction, especially around 200 Hz, which appear to indicate multiple mutually incoherent sources. Second, one-dimensional, equivalent-source-coherence properties at the jet centerline have been developed from the DAMAS-C beamforming algorithm. It has been shown for both engine conditions that the maximum source coherence occurs downstream of the maximum source level, which indicates that, as observed across the measurement array, the maximum source-level region is composed of both uncorrelated and correlated sources, and that the correlated source dominates farther downstream.

In conclusion, the cumulative results have provided a deeper understanding of jet-noise characteristics for a high-performance military aircraft, and provided connections to phenomena shown in the literature. The differences seen for the full-scale case may motivate further laboratory and computational investigations into understanding the physical mechanisms that result in these differences. By matching the coherence and correlation properties of the field, in addition to spectral levels, will result in more complete jet-noise models and possibly point toward efficient noise-reduction strategies.

Acknowledgments

The authors gratefully acknowledge the funding for this analysis from the Office of Naval Research. The measurements were funded by the U.S. Air Force Research Laboratory (USAFRL) through the Small Business Innovation Research program, and supported through a cooperative research and development agreement between Blue Ridge Research and Consulting, Brigham Young University, and the U.S. Air Force. This research was supported in part by the appointment of Blaine Harker to the Student Research Participation Program at USAFRL, 711th Human Performance Wing, Human Effectiveness Directorate, Warfighter Interface Branch, Battlespace Acoustics Branch administered by the Oak Ridge Institute for Science and Education through an interagency agreement between the U.S. Department of Energy and USAFRL. Distribution A: Approved for public release; distribution unlimited. 88ABW Cleared 23 April 2015; 88ABW-2015-2059.

References

- [1] Tam, C. K. W., Viswanathan, K., Ahuja, K. K., and Panda, J., "The Sources of Jet Noise: Experimental Evidence," *Journal of Fluid Mechanics*, Vol. 615, Nov. 2008, pp. 253–292.
doi:10.1017/S0022112008003704
- [2] Ahuja, K. K., Nance, D. K., Carrigan, J., and Karon, A., "On Coherence of Jet Noise," AIAA Paper 2014-2339, June 2014.
- [3] Tam, C. K., Pastouchenko, N. N., and Viswanathan, K., "Continuation of the Near Acoustic Field of a Jet to the Far Field. Part I: Theory," AIAA Paper 2010-3728, June 2010.
- [4] Tam, C. K. W., Viswanathan, K., Pastouchenko, N. N., and Tam, B., "Continuation of Near-Acoustic Fields of Jets to the Far Field: Part II Experimental Validation and Noise Source Characteristics," AIAA Paper 2010-3729, June 2010.
- [5] Viswanathan, K., Underbrink, J. R., and Brusniak, L., "Space-Time Correlation Measurements in Near Fields of Jets," *AIAA Journal*, Vol. 49, No. 8, 2011, pp. 1577–1599.
doi:10.2514/1.J050750
- [6] Harker, B. M., Gee, K. L., Neilsen, T. B., Wall, A. T., McNerny, S. A., and James, M. M., "On Autocorrelation Analysis of Jet Noise," *Journal of the Acoustical Society of America*, Vol. 133, No. 6, 2013, pp. EL458–EL464.
doi:10.1121/1.4802913
- [7] Wall, A. T., Gardner, M. D., Gee, K. L., and Neilsen, T. B., "Coherence Length as a Figure of Merit in Multireference Near-Field Acoustical Holography," *Journal of the Acoustical Society of America*, Vol. 132, No. 3, 2012, pp. EL215–EL221.
doi:10.1121/1.4740518
- [8] Michel, U., "The Role of Source Interference in Jet Noise," AIAA Paper 2009-3377, May 2009.
- [9] Reba, R., Narayanan, S., and Colonius, T., "Wave-Packet Models for Large-Scale Mixing Noise," *International Journal of Aeroacoustics*, Vol. 9, No. 4, 2010, pp. 533–558.
doi:10.1260/1475-472X.9.4-5.533
- [10] Miller, S. A., "Prediction of Near-Field Jet Cross Spectra," *AIAA Journal*, Vol. 53, No. 8, 2014, pp. 2130–2150.
doi:10.2514/1.J053614
- [11] Clarkson, B. L., "Correlation of Pressures Around a Jet Engine," *Proceedings of WADC University of Minnesota Conference on Acoustical Fatigue*, Wright Air Development Center TR-59-676, Wright-Patterson AFB, OH, March 1961, pp. 85–98.
- [12] Fuchs, H. V., "Space Correlations of the Fluctuating Pressure in Subsonic Turbulent Jets," *Journal of Sound and Vibration*, Vol. 23, No. 1, 1972, pp. 77–99.
doi:10.1016/0022-460X(72)90790-0
- [13] Fuchs, H. V., "Application of Acoustic Mirror, Telescope and Polar Correlation Techniques to Jet Noise Source Location," *Journal of Sound and Vibration*, Vol. 58, No. 1, 1978, pp. 117–126.
doi:10.1016/S0022-460X(78)80065-0
- [14] Maestrello, L., "Two-Point Correlations of Sound Pressure in the Far Field of a Jet: Experiment," NASA TM-X-72835, 1976.
- [15] Fisher, M. J., Harper-Bourne, M., and Glegg, S. A. L., "Jet Engine Noise Source Location: The Polar Correlation Technique," *Journal of Sound and Vibration*, Vol. 51, No. 1, 1977, pp. 23–54.
doi:10.1016/S0022-460X(77)80111-9
- [16] Ribner, H., "Two Point Correlations of Jet Noise," *Journal of Sound and Vibration*, Vol. 56, No. 1, 1978, pp. 1–19.
doi:10.1016/0022-460X(78)90566-7
- [17] Tam, C. K. W., "Influence of Nozzle Geometry on the Noise of High-Speed Jets," *AIAA Journal*, Vol. 36, No. 8, 1998, pp. 1396–1400.
doi:10.2514/3.13981
- [18] Tam, C. K. W., Golebiowski, M., and Seiner, J. M., "On the Two Components of Turbulent Mixing Noise from Supersonic Jets," AIAA Paper 1996-1716, May 1996.
- [19] Kumar, S. A., Karthikeyan, N., and Venkatakrishnan, L., "Correlation Studies in the Acoustic Far-Field of Non-Ideally Expanded Supersonic Jets," AIAA Paper 2013-2082, May 2013.
- [20] Liu, J., Corrigan, A. T., Kailasanath, K., Heeb, N. S., and Gutmark, E. J., "Numerical Study of Noise Sources Characteristics in an Under Expanded Jet Flow," AIAA Paper 2014-2604, June 2014.
- [21] Panda, J., Seasholtz, R. G., and Elam, K. A., "Investigation of Noise Sources in High-Speed Jets via Correlation Measurements," *Journal of Fluid Mechanics*, Vol. 537, No. 1, 2005, pp. 349–385.
doi:10.1017/S0022112005005148
- [22] Papamoschou, D., Morris, P. J., and McLaughlin, D. K., "Beamformed Flow-Acoustic Correlations in High-Speed Jets," AIAA Paper 2009-3212, May 2009.
- [23] Bendat, J. S., and Piersol, A. G., *Random Data: Analysis and Measurement Procedures*, 4th ed., Wiley, Hoboken, NJ, 2010, pp. 109–503.
- [24] Venkatesh, S. R., Polak, D. R., and Narayanan, S., "Beamforming Algorithm for Distributed Source Localization and Its Application to Jet Noise," *AIAA Journal*, Vol. 41, No. 7, 2003, pp. 1238–1246.
doi:10.2514/2.2092
- [25] Lee, S. S., and Bridges, J., "Phased-Array Study of Dual-Flow Jet Noise: Effect of Nozzles and Mixers," AIAA Paper 2006-2647, May 2006.
- [26] Schlinker, R., Liljenberg, S., Polak, D., Post, K., Chipman, C., and Stern, A., "Supersonic Jet Noise Source Characteristics & Propagation: Engine and Model Scale," AIAA Paper 2007-3623, May 2007.
- [27] Suzuki, T., and Colonius, T., "Instability Waves in a Subsonic Round Jet Detected Using a Near-Field Phased Microphone Array," *Journal of Fluid Mechanics*, Vol. 565, No. 1, 2006, pp. 197–226.
doi:10.1017/S0022112006001613
- [28] Harker, B. M., Gee, K. L., Neilsen, T. B., Wall, A. T., and James, M. M., "Phased-Array Measurements of Full-Scale Military Jet Noise," AIAA Paper 2014-3069, June 2014.
- [29] Dougherty, R. P., "Improved Generalized Inverse Beamforming for Jet Noise," *International Journal of Aeroacoustics*, Vol. 11, No. 3, 2012, pp. 259–290.
doi:10.1260/1475-472X.11.3-4.259
- [30] Sijtsma, P., "CLEAN Based on Spatial Source Coherence," *International Journal of Aeroacoustics*, Vol. 6, No. 4, 2007, pp. 357–374.
doi:10.1260/147547207783359459
- [31] Brooks, T. F., and Humphreys, W. M., "A Deconvolution Approach for the Mapping of Acoustic Sources (DAMAS) Determined from Phased Microphone Arrays," *Journal of Sound and Vibration*, Vol. 294, No. 4, 2006, pp. 856–879.
doi:10.1016/j.jsv.2005.12.046
- [32] Brooks, T. F., and Humphreys, W. M., Jr., "Extension of DAMAS Phased Array Processing for Spatial Coherence Determination (DAMAS-C)," AIAA Paper 2006-2654, May 2006.
- [33] Wall, A. T., Gee, K. L., James, M. M., Bradley, K. A., McNerny, S. A., and Neilsen, T. B., "Near-Field Noise Measurements of a High-Performance Military Jet Aircraft," *Noise Control Engineering Journal*, Vol. 60, No. 4, 2012, pp. 421–434.
doi:10.3397/1.3701021
- [34] Neilsen, T. B., Gee, K. L., Wall, A. T., and James, M. M., "Similarity Spectra Analysis of High-Performance Jet Aircraft Noise," *Journal of the Acoustical Society of America*, Vol. 133, No. 4, 2013, pp. 2116–2125.
doi:10.1121/1.4792360
- [35] Neilsen, T. B., Gee, K. L., and James, M. M., "Spectral Characterization in the Near and Mid-Field of Military Jet Aircraft Noise," AIAA Paper 2013-2191, 2013.
- [36] Liu, J., Corrigan, A. T., Kailasanath, K., and Taylor, B. D., "Multisource Statistically Optimized Near-Field Acoustical Holography," *Journal of the Acoustical Society of America*, Vol. 137, 2015, pp. 963–975.
doi:10.1121/1.4906585
- [37] Tam, C. K., and Parrish, S., "Noise of High-Performance Aircrafts at Afterburner," AIAA Paper 2014-2754, June 2014.
- [38] Wall, A. T., Gee, K. L., Neilsen, T. B., Harker, B. M., McNerny, S. A., McKinley, R. C., and James, M. M., "Investigation of Multi-Lobed Fighter Jet Noise Sources Using Acoustical Holography and Partial Field Decomposition Methods," AIAA Paper 2015-2379, June 2015.
- [39] Neilsen, T. B., Gee, K. L., Wall, A. T., James, M. M., and Atchley, A. A., "Comparison of Supersonic Full-Scale and Laboratory-Scale Jet Data and the Similarity Spectra for Turbulent Mixing Noise," *Proceedings of*

- Meetings on Acoustics*, Vol. 19, June 2013, Paper 040071.
doi:10.1121/1.4799664
- [40] Gee, K. L., Sparrow, V. W., James, M. M., Downing, J. M., Hobbs, C. M., Gabrielson, T. B., and Atchley, A. A., "The Role of Nonlinear Effects in the Propagation of Noise from High-Power Jet Aircraft," *Journal of the Acoustical Society of America*, Vol. 123, No. 6, 2008, pp. 4082–4093.
doi:10.1121/1.2903871
- [41] Wall, A., Gee, K., Neilson, T., Krueger, D., James, M., Sommerfeldt, S., and Blotter, J., "Full-Scale Jet Noise Characterization Using Scan-Based Acoustical Holography," AIAA Paper 2012-2081, June 2012.
- [42] Wall, A. T., Gee, K. L., Neilsen, T. B., McKinley, R. L., and James, M. M., "Military Jet Noise Source Imaging Using Multisource Statistically Optimized Near-Field Acoustical Holography," *Journal of the Acoustical Society of America* (submitted for publication).
- [43] Stout, T. A., Gee, K. L., Neilsen, T. B., Wall, A. T., and James, M. M., "Acoustic Intensity Near a High-Powered Military Jet Aircraft," *Journal of the Acoustical Society of America*, Vol. 138, No. 1, 2015, pp. EL1–EL7.
doi:10.1121/1.4934027
- [44] Morgan, J., Neilsen, T. B., Gee, K. L., Wall, A. T., and James, M. M., "Simple-Source Model of Military Jet Aircraft Noise," *Noise Control Engineering Journal*, Vol. 60, No. 4, 2012, pp. 435–449.
doi:10.3397/1.3701022
- [45] Neilsen, T., Gee, K., Harker, B., and James, M., "Level-Educed Wavepacket Representation of Noise Radiation from the F-22A Raptor," AIAA Paper 2016-1880, Jan. 2016.
- [46] Greska, B. J., "Supersonic Jet Noise and Its Reduction Using Microjet Injection," Ph.D. Dissertation, Florida State Univ., Tallahassee, FL, 2005.
- [47] Baars, W. J., Tinney, C. E., Murray, N. E., Jansen, B. J., and Panickar, P., "The Effect of Heat on Turbulent Mixing Noise in Supersonic Jets," AIAA Paper 2011-1029, Jan. 2011.
- [48] Seiner, J., Jansen, B., and Ukeiley, L., "Acoustic Fly-Over Studies of F/AE/F Aircraft During FCLP Mission," AIAA Paper 2003-3330, May 2003.
- [49] Krothapalli, A., Venkatakrishnan, L., and Lourenco, L., "Crackle: A Dominant Component of Supersonic Jet Mixing Noise," AIAA Paper 2000-2024, June 2000.
- [50] Baars, W. J., and Tinney, C. E., "Shock-Structures in the Acoustic Field of a Mach 3 Jet with Crackle," *Journal of Sound and Vibration*, Vol. 333, No. 12, 2014, pp. 2539–2553.
doi:10.1016/j.jsv.2014.01.008
- [51] Seiner, J. M., Ponton, M. K., Jansen, B. J., and Lagen, N. T., "The Effects of Temperature on Supersonic Jet Noise Emission," *Proceedings of the 14th DGLR/AIAA Aeroacoustics Conference*, AIAA Paper 92-02-046, May 1992, pp. 295–307.
- [52] Tam, C. K. W., and Zaman, K. B. M. Q., "Subsonic Jet Noise from Nonaxisymmetric and Tapped Nozzles," *AIAA Journal*, Vol. 38, No. 4, 2000, pp. 592–599.
doi:10.2514/3.14449
- [53] Jordan, P., and Colonius, T., "Wave Packets and Turbulent Jet Noise," *Annual Review of Fluid Mechanics*, Vol. 45, Jan. 2013, pp. 173–195.
doi:10.1146/annurev-fluid-011212-140756
- [54] Harker, B. M., Neilsen, T. B., Gee, K. L., James, M. M., and Wall, A. T., "Spatiotemporal Correlation Analysis of Jet Noise from a High-Performance Military Aircraft," AIAA Paper 2015-2376, June 2015.
- [55] Viswanathan, K., "Mechanisms of Jet Noise Generation: Classical Theories and Recent Developments," *International Journal of Aeroacoustic*, Vol. 8, No. 4, 2009, pp. 355–407.
doi:10.1260/147547209787548949
- [56] Wall, A. T., Gee, K. L., and Neilsen, T. B., "Multisource Statistically Optimized Near-Field Acoustical Holography," *Journal of the Acoustical Society of America*, Vol. 137, No. 2, 2015, pp. 963–975.
doi:10.1121/1.4906585

P. D. Papamoschou
Associate Editor